

¹H NMR Study of Hydrogen Abstraction in Model Compound Mimics of Polymers[†]

Jeffrey R. Lancaster^{1,2}, Rachael Smilowitz², Nicholas J. Turro^{1,2} and Jeffrey T. Koberstein^{*2}

¹Department of Chemistry, Columbia University, New York, NY

²Department of Chemical Engineering, Columbia University, New York, NY

Received 15 August 2013, accepted 6 November 2013, DOI: 10.1111/php.12214

ABSTRACT

Small molecules representing common synthetic polymers were subjected to photochemically induced hydrogen abstraction by benzophenone. Reactions were monitored using ¹H NMR to query the factors that influence preferential abstraction of protons in unique chemical environments. Differences in bond dissociation energies do not fully explain the observed hydrogen abstraction preferences. To that end, we identify contributions to abstraction from prereactive complexation, radical stability, steric effects and charge transfer effects. Using representative small molecule model compounds in lieu of polymeric materials is a novel approach to understanding photochemical reaction in polymers; however, it cannot probe the contributions of macromolecular effects—e.g. polymer rigidity or side chain and backbone mobility—to preferential hydrogen abstraction.

INTRODUCTION

Photoactive moieties are routinely used to modify the properties of polymers in a host of applications ranging from postpolymerization modifications such as photoaffinity labeling of biopolymers, photocross-linking and photodegradation, to the initial synthesis of the polymers themselves by photoinitiation. All of these methods are based on the action of photoexcited molecules upon large, structurally complex molecules (1). The versatility and importance of photoactive compounds such as benzophenone, phthalimide, xanthone, sulfonyl azide, phenyl azide and ortho-nitrobenzyl alcohols provide an overarching need to better understand the mechanism of their interactions with the polymers they modify.

Benzophenone, in particular, is one of the most well-studied and well-behaved photoactive compounds, and has variously been used as a triplet sensitizer, a hydrogen abstractor and a polymerization initiator (2,3).

The process of hydrogen abstraction by benzophenone shown in Scheme 1 is well understood (4). To a first approximation, the rate and extent of the reaction of excited benzophenone with any hydrogen donor ought to depend primarily on the energy of the excited benzophenone and the bond strength of the X–H bond that is broken during the rate determining step (r.d.s. in Scheme 1). As the triplet energy of benzophenone is constant, we would expect hydrogen atoms in similar chemical environ-

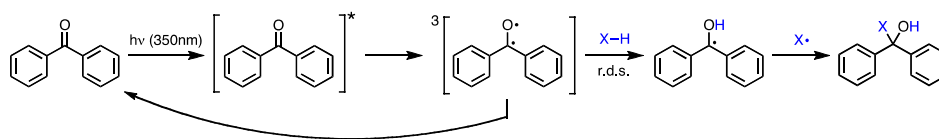
ments to have similar reactivity toward photoexcited benzophenone (5).

Previous work from our group focused on the use of benzophenone as a hydrogen abstraction agent to induce cross-linking within a polymer film to inhibit dewetting (6). We have also compared the efficacies of mono-functional benzophenone and a difunctional bis-benzophenone compound for cross-linking a variety of polymers (7). In the latter work, we found that the details of the cross-linking mechanism were dependent on the nature of the polymer studied. In polystyrene, cross-linking was accompanied by considerable main chain scission, whereas in poly(*n*-butyl acrylate), almost no main chain scission was observed. We concluded that the underlying hydrogen abstraction mechanism leading to cross-linking must depend on the polymer structure. In the case of polystyrene, we postulated that hydrogen abstraction and thus macroradical formation occurs primarily on the polymer chain backbone, thus facilitating main chain scission reactions. In poly(*n*-butyl acrylate), on the other hand, we surmised that hydrogen abstraction and thus radical formation must occur primarily on the polymer side chains so that scission reactions can break only the side chain, thus accounting for the lack of significant main chain scission of the polymer backbone. As the manifestation of main chain scission decreases the molecular weight and is therefore undesirable, these results provided strong motivation to study the hydrogen abstraction mechanism in polymers and how it depends upon the molecular structure of the polymeric repeat unit. Toward that end, we examine herein the ability of photoexcited benzophenone to abstract hydrogen atoms from model compounds that have been selected to represent commonly used polymers. Proton nuclear magnetic resonance spectroscopy was used to determine the relative likelihood of abstraction of each of the different hydrogen atoms in these model compounds.

Species other than triplet benzophenone have also been used to examine hydrogen atom abstraction processes including *tert*-butoxy, chlorine and hydroxy radicals (8–10), but the aim of the present work was to develop a framework for understanding—and possibly predicting and controlling—how and where on a polymer molecule the photochemical reaction of benzophenone will take place. Attaining this goal is complicated, as the hydrogen abstraction mechanism is most likely influenced by a number of factors besides molecular structure, including, but certainly not limited to, bond strengths, local molecular mobility, steric hindrance, confinement and other macromolecular and supramolecular effects.

*Corresponding author email: jk1191@columbia.edu (Jeffrey T. Koberstein)

[†]This paper is part of the Special Issue honoring the memory of Nicholas J. Turro
© 2013 The American Society of Photobiology



Scheme 1. Excitation of benzophenone and subsequent hydrogen abstraction from a hydrogen donor (X-H).

MATERIALS AND METHODS

¹H NMR of model compounds. ¹H NMR was used to monitor the extent of hydrogen abstraction reactions as the technique can measure the transfer of hydrogen atoms between different chemical environments. To simplify interpretation of the ¹H NMR spectra, we have chosen to study a series of model compounds with structures that mimic the repeat units of a number of commonly used polymers. The manner in which the structures of the model compounds map onto those of commonly used polymers is shown in Table 1 (11–15). For instance, caprolactam (**1**) was used as a small molecule substitute for polycaprolactam, and ϵ -caprolactone (**3**) was used for polycaprolactone. The selection of model compounds in Scheme 2 was based on both their similarity to target polymers and their commercial availability.

In the selection process, it was important to realize that the behavior of the polymer is not always chemically well represented by its monomer. For instance, the energy of the bond α to the aromatic ring of styrene monomer is $\sim 115 \text{ kcal mol}^{-1}$, whereas the same bond in ethylbenzene—a compound with bonds more like those in polystyrene—is $\sim 100 \text{ kcal mol}^{-1}$ (Scheme 3). The hybridization and conjugation of the styrene vinyl group affect both the C–C and the C–H bond energies at α and β positions relative to the phenyl ring. Therefore, instead of using its monomer styrene, we chose *sec*-butylbenzene (**4**) and ethylbenzene (**5**) as the model compounds that will best represent the behavior of hydrogen atoms in polystyrene.

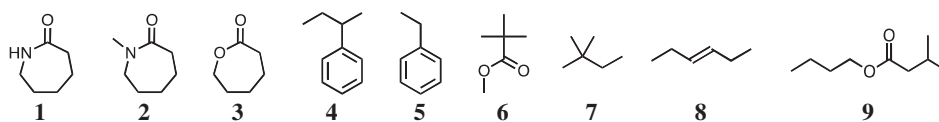
Other compounds were chosen that closely resembled the repeat units of polymers, or that were nearly analogous to the polymer structure. Methyl trimethylacetate (**6**) and butyl isovalerate (**9**) were chosen to represent poly(*tert*-butyl acrylate) and poly(*n*-butyl acrylate), respectively. Hydrocarbons 2,2-dimethylbutane (**7**) and trans-3-hexene (**8**) were chosen to mimic polymers such as branched polyethylene and polybutadiene.

Experimental details. Benzophenone (Acros Organics), caprolactam (Sigma Aldrich, **1**), methylcaprolactam (Sigma Aldrich, **2**), ϵ -caprolactone (Sigma Aldrich, **3**), *sec*-butylbenzene (Alfa Aesar, **4**), ethylbenzene (Sigma Aldrich, **5**), methyl trimethylacetate (Sigma Aldrich, **6**), 2,2-dimethylbutane (Sigma Aldrich, **7**), trans-3-hexene (Sigma Aldrich, **8**), butyl isovalerate (SAFC, **9**), and CD₃CN (Cambridge Isotopes & Acros Organics) were used as received. Solutions were irradiated in a Rayonet reactor (16 lamps, $\sim 4.5 \text{ W}$ each, The Southern New England Ultraviolet Company) at 350 nm. ¹H NMR spectra were recorded on a Bruker Spectrospin 300 MHz spectrometer.

Benzophenone (*ca* 4 mg) was dissolved in 6 mL of an approximately 90 mM solution of model compound (**1–9**) in CD₃CN. The solution was transferred to a quartz tube capable of being inserted into a standard NMR tube, and inert gas was bubbled through the solution for 5 min to remove oxygen. The quartz tube was sealed with a cap and Parafilm, placed into a standard NMR tube and a ¹H NMR spectrum was recorded. The quartz tube was irradiated at 350 nm for up to 3 h; periodically during irradiation the quartz tube was removed from the reactor, reinserted

Table 1. Structural comparison of selected polymers and model compounds.

Polymer	Model Compounds
	 Caprolactam, 1
	 ϵ -Caprolactone, 3
	 <i>sec</i> -Butylbenzene, Ethylbenzene, 5
	 Methyl trimethylacetate, 6
	 trans-3-Hexene, 8
	 Butyl isovalerate, 9



Scheme 2. Structures of the compounds used in this study: caprolactam, 1; methyl-caprolactam, 2; caprolactone, 3; *sec*-butylbenzene, 4; ethylbenzene, 5; methyl trimethylacetate, 6; 2,2-dimethylbutane, 7; trans-3-hexene, 8; and butyl isovalerate, 9.



Scheme 3. Comparison of C–C bond dissociation energies in ethylbenzene, 5, and styrene.

into the NMR tube and ^1H NMR spectra were recorded. NMR spectra were processed using MestReNova software.

RESULTS

^1H NMR analysis

A set of ^1H NMR spectra recorded for compound **1** is shown in Fig. 1 and is representative of each model compound tested (see Supplementary Materials for all ^1H NMR spectra and analyses, Figures and Tables S1–S9). The benzophenone C–H peaks (δ 7.0–8.0) are generally well separated from the proton signals of the model compounds, except in the case of compounds that contain aromatic hydrogen atoms (4,5). As the sample was irradiated at 350 nm, the peaks corresponding to benzophenone (δ 7.5–8.0) and the model compound decreased in intensity, while new peaks (δ 7.0–7.6, others) corresponding to the reaction products increased in intensity.

To quantitatively analyze the relative rates of decrease in each model compound X–H signal, the spectra were calibrated to a constant integral in the range δ 7.0–8.0. Control experiments indicated that benzophenone does not react with itself in CD_3CN , and therefore the number of aromatic hydrogens from the benzophenone remains constant as an internal standard. In addition, benzophenone did not react with the CD_3CN and the model compounds alone in CD_3CN did not react when irradiated. No decrease greater than 6% was found in the control experiments

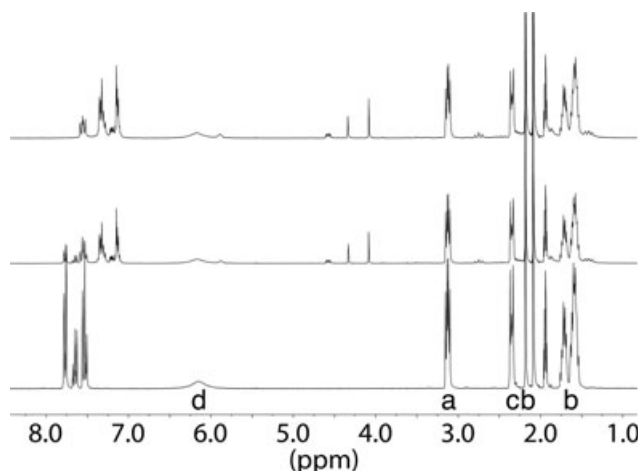


Figure 1. 300 MHz ^1H NMR spectra of a 96.9 mM solution of **1** (CD_3CN) and benzophenone after 0 min (bottom), 30 min (middle) and 120 min (top) irradiation at 350 nm.

indicating that both benzophenone and the model compound must be present for a photochemically induced reaction to occur. In cases where the signals from aromatic hydrogens of a model compound overlap the benzophenone region, the entire spectrum was calibrated under the assumption that the total number of hydrogen atoms in the solution remained constant. In cases where a water impurity peak overlaps with a model compound proton signal, the water peak was fit with a Lorentzian function to subtract its overlap. Once scaled appropriately, difference spectra were generated (Fig. 2) to visualize the relative decreases of the initial model compound proton signals in comparison to the growth of new signals from the reaction products.

Samples were irradiated until either the initial benzophenone peaks had shifted completely to the characteristic product peaks (Fig. 1, δ 7.0–7.6) or until the benzophenone peaks no longer decreased with increased irradiation time indicating the reaction was complete. Integrals of each region were normalized to the integral at $t = 0$. The resulting values are plotted in Fig. 3 for model compound **1**. The integrals for each type of hydrogen atom were fit according to an exponential decay expected for a first-order rate mechanism (Eq. 1 and Fig. 3, dotted lines), where t is the irradiation time in minutes. The values of the exponential coefficients, k , are collected in Table 2.

$$y = Ae^{-kt} + C \quad (1)$$

DISCUSSION

Bond dissociation energies

As shown in Scheme 1, photochemically induced hydrogen abstraction by benzophenone is initiated by photoexcitation of an electron pair from the singlet ground state to first singlet excited

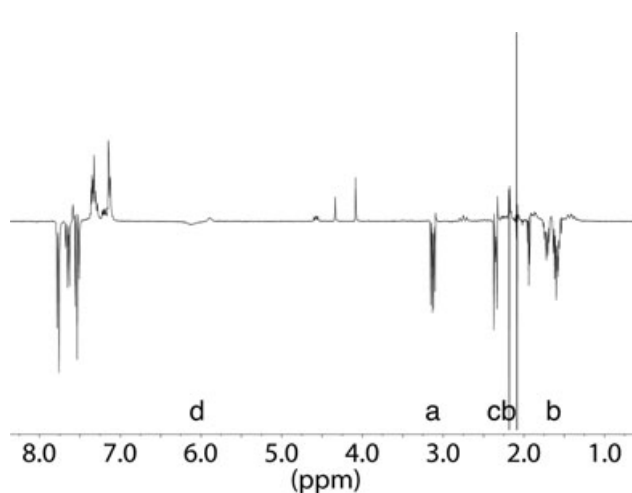


Figure 2. Difference between 300 MHz ^1H NMR spectra of **1** (CD_3CN) and benzophenone before and after 120 min irradiation at 350 nm.

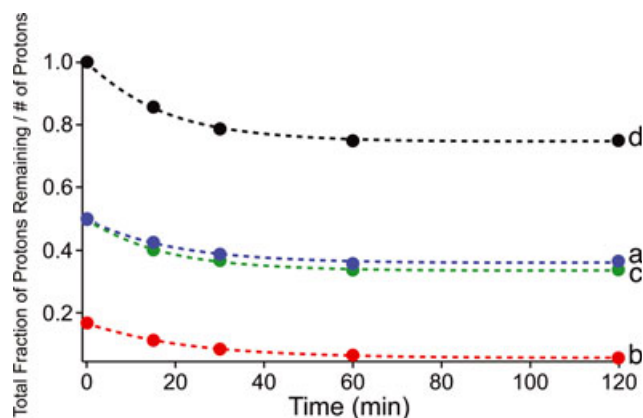


Figure 3. Plot of ^1H NMR integrals for protons a–d of compound **1** scaled by initial integral and number of protons with increasing irradiation time. Each set of data points is fit with Eq. 1.

Table 2. Values of k using Eq. 1 to fit the data in Fig. 3 for **1**.

	H_a	H_b	H_c	H_d
k	0.053 ± 0.008	0.045 ± 0.009	0.060 ± 0.003	0.058 ± 0.004

n, π^* state, which is quickly followed by an intersystem crossing to the triplet state. The triplet state, a diradical with one oxygen-centered radical and one carbon-centered radical, can either decay to the ground state or the oxygen-centered radical can abstract a hydrogen atom from a nearby molecule. The resulting pair of radicals can then either recombine to generate a covalent bond, can transfer the hydrogen back to its original location, or can undergo subsequent radical reactions. For simplicity, an energy state diagram that considers only the pathway toward recombination will elucidate the role of bond dissociation energy in the hydrogen abstraction preferences of benzophenone.

The relative energies of the starting materials (benzophenone, BP and substrate, S) and the recombination product of photoinduced hydrogen abstraction are shown schematically in Fig. 4. The singlet n, π^* state of benzophenone is $75.5 \text{ kcal mol}^{-1}$ higher in energy than the ground state and is not shown because the singlet undergoes complete intersystem crossing to the triplet ($68.6 \text{ kcal mol}^{-1}$) with a quantum yield of unity ($\Phi_T = 1$) (16). The gray lines in Fig. 4 represent a range of possible values of the energy of the hydrogen abstraction products—diphenyl alcohol radical and the substrate radical—that depend on the energy of the X–H bond that is broken since each O–H bond formed is identical. The last step in this process is recombination of the two radicals to generate a new X–C bond. Energies for the O–H, C–C and N–C bonds formed can be estimated as 102, 75 and 65 kcal mol^{-1} , respectively, to give a range of the possible X–H bond energies that would be made the overall reaction exothermic ($\Delta H_{\text{rxn}} < 0$) (17–19). Substituting the known or estimable energies into Eq. 2 gives the upper limit of X–H bond energy that will undergo an exothermic hydrogen abstraction by benzophenone to be $108 \text{ kcal mol}^{-1}$. An additional limit is placed upon the reaction in order for the rate of hydrogen abstraction to be competitive with deactivation of the excited benzophenone. There must be little to no activation energy barrier to the

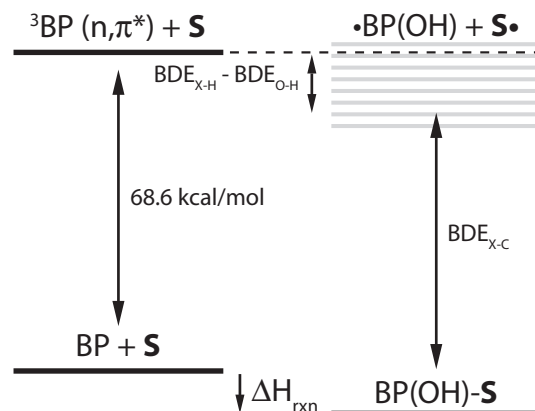


Figure 4. Energy state diagram for hydrogen abstraction by benzophenone (BP) from a substrate, S, followed by recombination.

formation of the hydrogen abstraction products during the rate-determining step, so the hydrogen abstraction step must also be exothermic (4). Taking this into account makes the upper limit of X–H bond energy approximately $102 \text{ kcal mol}^{-1}$.

$$\begin{aligned} \Delta H_{\text{rxn}} &= [E(^3\text{BP}_{n,\pi^*}) + \text{BDE}_{\text{X-H}}] - [\text{BDE}_{\text{O-H}} + \text{BDE}_{\text{X-C}}] \\ &= \left[68.6 \frac{\text{kcal}}{\text{mol}} + \text{BDE}_{\text{X-H}} \right] - \left[102 \frac{\text{kcal}}{\text{mol}} + 75 \frac{\text{kcal}}{\text{mol}} \right] \quad (2) \end{aligned}$$

$$\Delta H_{\text{rxn}} < 0 \text{ when } \text{BDE}_{\text{X-H}} \leq 108 \frac{\text{kcal}}{\text{mol}}$$

The majority of the X–H bond dissociation energies of the model compounds **1–9** have not been measured or tabulated, so it is necessary to consult tables of representative compounds to infer relative bond dissociation energies (17–20). Representative compounds for the X–H bonds of **1**, their bond dissociation energies and their relationships to **1** are shown in Table 3 along with the value of k determined experimentally for each X–H bond. For compounds **1–9**, the X–H bond energies of most of the representative compounds are significantly lower than $102 \text{ kcal mol}^{-1}$, indicating that each ought to be abstractable by excited benzophenone. The only representative bond dissociation energies that fall outside the thermodynamically acceptable range of X–H bond energies are the N–H bond of **1** ($109.5 \text{ kcal mol}^{-1}$) and the alkenyl C–H of **8** (*ca* $110 \text{ kcal mol}^{-1}$). Based on thermodynamics alone, we would expect no abstraction of these two hydrogen atoms by excited benzophenone.

Directly and quantitatively comparing tabulated bond dissociation energies is problematic, however, because of the wide variety of methods used to determine bond dissociation energies: shock tube techniques, laser flash photolysis, correlation methods, etc. (17–22). A more holistic experimental method, such as the one used here, samples all X–H bonds simultaneously and provides a comprehensive picture of the competitive relationships between various X–H bonds within the same molecule without needing to directly measure bond dissociation energies.

Other influences

Differences in bond dissociation energy alone do not account for the preferential abstraction of particular hydrogen atoms from compounds **1–9** by benzophenone. Table 3 shows that the alkyl

Table 3. Compounds with representative bond dissociation energies for the hydrogen atoms of **1**, the relation of each representative bond to **1** and the competitive rate value of k/k_a scaled for the number of hydrogen atoms.

Representative compound	X-H BDE (kcal/mol)	Relation to 1	k/k_a
N,N-dimethylacetamide	91.0*	H_a	1
cycloheptane	93.3 [†] 94.0 [‡] 92.5 [§] 96.5	H_b	0.28
N-isopropylacetamide	93.1*	H_c	1.13
2-piperidone	109.5	H_d	2.19

Methods for determination of bond dissociation energies: *Correlation; [†]Polanyi correlation; [‡]Kinetics; [§]Photobromination; ^{||}Intersecting parabolas; ^{||}Acidity-oxidation potential measurement.

C–H bonds (H_a , H_b , H_c) of **1** have similar bond dissociation energies in the range 91–96 kcal mol^{−1} but are not abstracted at the same rate. The N– H_d bond is the most likely to be abstracted, however, despite being approximately 15 kcal mol^{−1} higher in energy than the C– H_a , C– H_b and C– H_c bonds. The larger-than-expected rate for H_d can be explained by the formation of a prereactive hydrogen-bonded complex between the N–H bond and a lone pair of electrons on the carbonyl oxygen of benzophenone. By bringing the reactive end of the benzophenone close to the amine hydrogen, the number of abstraction events from that position is increased relative to abstraction based on bond energies alone. In addition, prereactive complexation weakens the N–H bond, making it more susceptible to abstraction. Such an effect is not seen for **2** which lacks a nitrogen-centered hydrogen atom with which to hydrogen bond. The hydrogen atoms bonded to carbon atoms next to the amide of **1** and of **2** are roughly equally preferred sites for abstraction,

whereas the alkyl C–H bonds are deactivated to abstraction relative to the other available hydrogen atoms.

Comparison with what is known for another high bond energy C–H bond supports the notion of prereactive complexation of benzophenone and **1**. The alkenyl C–H of **8** has high bond dissociation energy (*ca* 110 kcal mol^{−1}) due to the sp^2 hybridization of the carbon atom, but it cannot form a complex with the benzophenone. The rate of abstraction from the alkenyl C–H bond is less than the rate of abstraction from the alkyl C–H bonds (H_b , H_c) as would be expected (Table 4). It is worth noting that the hydrogen atoms on the carbon atom positioned α to the double bond are abstracted more readily than the terminal methyl protons, likely due to the resonance stabilization provided to the radical by the double bond.

Radical stability plays a role in the hydrogen abstraction preferences in compounds such as **4**, **5** and **7**. In each case, as expected, tertiary hydrogen atoms are abstracted preferentially—relative to the number of hydrogens available—followed by secondary and primary hydrogen atoms. According to these data, secondary hydrogen atoms are abstracted roughly three to four times as often as primary hydrogen atoms (**5**, **7**), and roughly half as often as tertiary hydrogen atoms (**4**). Some balance is achieved in the compounds studied as there are generally more primary hydrogen atoms available than secondary hydrogen atoms, and more secondary hydrogen atoms available than tertiary hydrogen atoms.

Aside from bond dissociation energy and radical stability, steric effects and polar or charge transfer effects can influence the relative abstraction of hydrogen atoms by excited benzophenone. Steric effects play a clear role in the hydrogen abstraction preferences of **6**; the hydrogen atoms of compound **6** have comparable bond dissociation energies within 2.5 kcal mol^{−1}, however, the *tert*-butyl hydrogen atoms (H_b) were abstracted nearly twice as much as the methyl ester hydrogen atoms (H_a) (Table 5). This implies that peripheral hydrogens that can freely sample the solvent volume around a molecule are more likely to be accessed by excited benzophenone. Hydrogen atoms hidden in the interiors of molecules are less accessible, and therefore are abstracted less often despite having similar bond dissociation energies. This conclusion validates our previous postulate that side chain hydrogens are preferentially abstracted in poly(*n*-butyl acrylate) compared to main chain hydrogens (**7**).

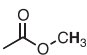
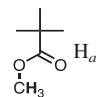
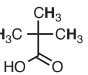
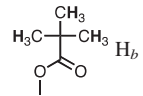
Contributions from polar or charge transfer effects on the linear transition state of the approaching radical must also be con-

Table 4. Compounds with representative bond dissociation energies for the hydrogen atoms of **8**, the relation of each representative bond to **8** and the competitive rate value of k/k_a scaled for the number of hydrogen atoms.

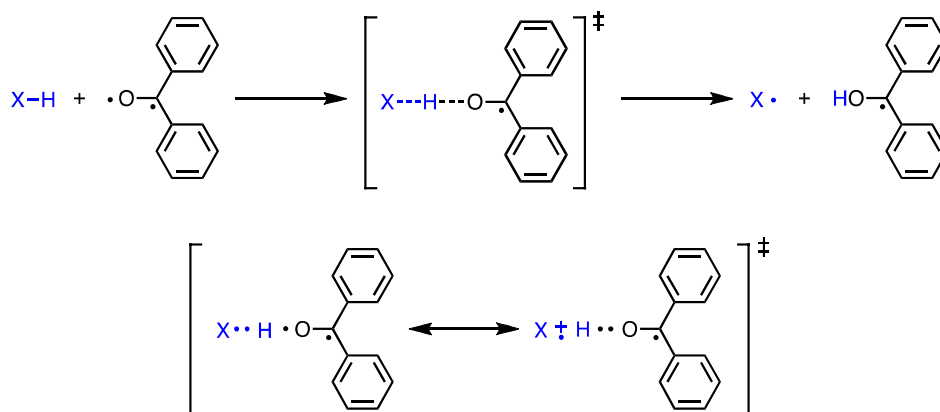
Representative compound	X-H BDE (kcal/mol)	Relation to 8	k/k_a
Propene	109 ± 2.4* 111.1*	H_a	1
(<i>E</i>)-2-pentene	81.7 ± 1.5 [†] 82.5 [‡]	H_b	3.13
Butane	101 ± 2 [§] 100.2 100.7* 101.7 ± 0.5	H_c	2.08

Methods for determination of bond dissociation energies: *Single-pulse shock tube technique; [†]Derived from ΔH_f° ; [‡]Correlation; [§]Electron impact; ^{||}Appearance energy measurements; ^{||}Photoionization mass spectrometry.

Table 5. Compounds with representative bond dissociation energies for the hydrogen atoms of **6**, the relation of each representative bond to **6** and the competitive rate value of k/k_a scaled for the number of hydrogen atoms.

Representative compound	X-H BDE (kcal mol ⁻¹)	Relation to 6	k/k_a
Acetic acid methyl ester 	96.7*		1
2,2-dimethyl- propanoic acid 	99.2*		2.22

Methods for determination of bond dissociation energies: *Correlation.

**Scheme 4.** Resonance structure (bottom) showing possible polar effects during the transition state (top) of hydrogen abstraction from X-H by triplet benzophenone.

sidered (10). In cases where an alkyl C-H bond is to be broken, the polar diradical is neither stabilized nor destabilized during the transition state according to the resonance structure shown in Scheme 4, and polarity effects are expected to be insignificant. In other cases, a polar group—*e.g.* an ester or amide—may direct the incoming radical toward particular positions on the structure; chlorine radicals are directed to the β position of propionic acid, whereas nonpolar alkyl and phenyl radicals are directed to the α position. In compound **3**, the ester directs the incoming benzophenone radicals to the ω position (H_c , 6 position for **3**) next to the ethereal oxygen of the ester. Reaction at that position is nearly five times greater than reaction at the α position (H_a) or the β - δ positions (collectively H_b). Amides seem to instead direct equally to the α and ω positions, as shown for compounds **1** and **2**.

Building a predictive framework: Hydrogen abstraction from proteins and polymers

A predictive framework for the differences in hydrogen atom reactivity toward abstraction by benzophenone identified by ¹H NMR cannot be based solely on differences in bond dissociation energies when the X-H bonds are below the threshold for abstraction. As most of the X-H bond dissociation energies fall in a similar thermodynamic range, factors that influence the kinetics of the reaction must dominate these hydrogen abstraction reactions. Sterics of side chains and polymer backbones, solvent

accessibility, backbone flexibility, radical stability, hydrogen bonding prereactive complexation and polarity effects will therefore likely play an increased role in determining abstraction preferences when these reactions occur in thin polymer films as opposed to in solution. In addition, hydrogen atoms may be more or less accessible, mobile and susceptible to attack by excited benzophenone depending on whether the polymer is in a melt or glassy state.

While this is the first study of these interactions using model compounds representative of synthetic polymers, other studies have found similar results when examining model compounds representative of biopolymers. A series of amino acids with aliphatic and carboxylic- or ammonium-functional side chains was subjected to hydrogen abstraction by chlorine photolyzed in trifluoroacetic acid (23). As expected, the rate of abstraction of tertiary hydrogens (CH) was found to be greater than the rate of abstraction of methylene hydrogen atoms (CH₂), which in turn was greater than the reactivity of hydrogen atoms in methyl groups (CH₃). Unexpectedly, however, the rate of abstraction was found to be greater for hydrogen atoms farther away from the amino acid backbone. This effect was attributed to the repulsion of an incoming radical by the carboxyl and cationic amino functionalities in the small molecules, and was extrapolated to represent the effect of the amido linkage in the polyamide backbone upon hydrogen abstraction from proteins (10).

A computational examination of hydrogen abstraction from amino acids stressed the various kinetic factors that contribute to

radical preferences (24). Prereactive complexation of a hydroxyl radical with amino and carbonyl groups, solvent accessibility and the diminished role of bond dissociation energies are all considered to contribute to the preferences of a hydrogen-abstracting radical. The authors of that study also hypothesized that the increased reactivity of hydrogen atoms located farther from the amino acid backbone is due to the greater flexibility of those side chains relative to the more rigid backbone.

The polymers represented by the compounds considered in this study (Table 1) fall into two categories: those with aliphatic backbones, and those with amido- and ester-functional backbones. Based on the amino acid work described above, we would expect a number of differences between the model compounds studied and their polymeric counterparts. First, the model compounds **1–3** retain the functionality that ultimately is present in the backbone of the polymer, whereas the amino acids bear charged endgroups that do not accurately represent the protein amido linkages. As the amido and ester groups of compounds **1–3** are isoelectronic with their representative polymers, we would expect no difference between the roles played by the amide and ester in **1–3** and their role in the parent polymers. For the remaining model compounds that represent polymers with aliphatic backbones, we would expect no difference from electronic effects since neither the model compound nor the polymer backbone is charged.

For the polymers represented by compounds **1–3** where direction by amide and ester linkages may still occur, we might expect hydrogen atoms adjacent to the linkages to be most readily abstracted if any effect at all is observed in the polymer. The absence of electronic diversity in the aliphatic backbones of the synthetic polymers represented by model compounds **4–9** should obviate the charge transfer effects and distance-dependent effects observed in proteins. We would not expect to observe an increased rate of hydrogen abstraction for side chain hydrogen atoms located farther from the polymer backbone because of repulsive effects from the aliphatic backbone.

We might, however, expect the difference in rigidity between the side chains and the polymer backbone to have some influence. The model compounds **1–9** lack distinct regions of rigidity that would be present in the polymers they represent. The sections of the model compounds that represent the backbone of the parent polymers are not restricted in any way, and therefore do not accurately account for how a polymer side chain may sample space relative to the backbone. As polymer chains can only move by rotation about bonds, side chains naturally rotate around the polymer backbone and can thereby effectively shield an approaching benzophenone molecule from reaching C–H bonds on the chain backbone. Although the bond energies of the model compounds may be analogous to those found in polymers, the motion, accessibility and shape of a polymer chain are not well represented by the model compounds.

Acknowledgements—This material is based upon work supported by the National Science Foundation under grant DMR-0704054. JRL was supported by fellowships provided by National Science Foundation grant IGERT-0221589 and DGE-0742450.

SUPPORTING INFORMATION

Additional Supporting Information may be found in the online version of this article:

Figure S1. (a) 300 MHz ^1H NMR spectra of a 96.9 mM solution of **1** (CD_3CN) after 0 min (bottom), 30 min (middle) and 120 min (top) (b). Difference between 300 MHz ^1H NMR spectra of **1** (CD_3CN) before and after 120 min irradiation at 350 nm (c) Plot of decreasing ^1H NMR integrals scaled by initial integral and number of protons with increasing irradiation time of **1**. Each set of data is fit by $y = Ae^{-kt} + C$.

Figure S2. (a) 300 MHz ^1H NMR spectra of a 92.3 mM solution of **2** (CD_3CN) after 0 min (bottom), 30 min (middle) and 120 min (top) (b) Difference between 300 MHz ^1H NMR spectra of **2** (CD_3CN) before and after 120 min irradiation at 350 nm (c) Plot of decreasing ^1H NMR integrals scaled by initial integral and number of protons with increasing irradiation time of **2**. Each set of data is fit by $y = Ae^{-kt} + C$.

Figure S3. (a) 300 MHz ^1H NMR spectra of a 95.7 mM solution of **3** (CD_3CN) after 0 min (bottom), 30 min (middle) and 120 min (top) (b) Difference between 300 MHz ^1H NMR spectra of **3** (CD_3CN) before and after 120 min irradiation at 350 nm (c) Plot of decreasing ^1H NMR integrals scaled by initial integral and number of protons with increasing irradiation time of **3**. Each set of data is fit by $y = Ae^{-kt} + C$.

Figure S4. (a) 300 MHz ^1H NMR spectra of an 88.6 mM solution of **4** (CD_3CN) after 0 min (bottom), 30 min (middle) and 120 min (top). Signals from the aromatic protons of **4** overlap adduct proton signals in the region $\delta 7.0\text{--}7.4$ (b) Difference between 300 MHz ^1H NMR spectra of **4** (CD_3CN) before and after 120 min irradiation at 350 nm. Signals from the aromatic protons of **4** overlap adduct proton signals in the region $\delta 7.0\text{--}7.4$ (c) Plot of decreasing ^1H NMR integrals scaled by initial integral and number of protons with increasing irradiation time of **4**. Each set of data is fit by $y = Ae^{-kt} + C$.

Figure S5. (a) 300 MHz ^1H NMR spectra of an 81.7 mM solution of **5** (CD_3CN) after 0 min (bottom), 30 min (middle) and 120 min (top). Signals from the aromatic protons of **5** overlap adduct proton signals in the region $\delta 7.0\text{--}7.4$ (b) Difference between 300 MHz ^1H NMR spectra of **5** (CD_3CN) before and after 120 min irradiation at 350 nm. Signals from the aromatic protons of **5** overlap adduct proton signals in the region $\delta 7.0\text{--}7.4$ (c) Plot of decreasing ^1H NMR integrals scaled by initial integral and number of protons with increasing irradiation time of **5**. Each set of data is fit by $y = Ae^{-kt} + C$.

Figure S6. (a) 300 MHz ^1H NMR spectra of an 81.4 mM solution of **6** (CD_3CN) after 0 min (bottom), 120 min (middle) and 360 min (top) (b) Difference between 300 MHz ^1H NMR spectra of **6** (CD_3CN) before and after 360 min irradiation at 350 nm (c) Plot of decreasing ^1H NMR integrals scaled by initial integral and number of protons with increasing irradiation time of **6**. Each set of data is fit by $y = Ae^{-kt} + C$.

Figure S7. (a) 300 MHz ^1H NMR spectra of a 98.6 mM solution of **7** (CD_3CN) after 0 min (bottom), 30 min (middle) and 120 min (top) (b) Difference between 300 MHz ^1H NMR spectra of **7** (CD_3CN) before and after 120 min irradiation at 350 nm (c) Plot of decreasing ^1H NMR integrals scaled by initial integral and number of protons with increasing irradiation time of **7**. Each set of data is fit by $y = Ae^{-kt} + C$.

Figure S8. (a) 300 MHz ^1H NMR spectra of an 85.2 mM solution of **8** (CD_3CN) after 0 min (bottom), 30 min (middle) and 60 min (top) (b) Difference between 300 MHz ^1H NMR spectra of **8** (CD_3CN) before and after 60 min irradiation at 350 nm (c) Plot of decreasing ^1H NMR integrals scaled by initial integral and number of protons with increasing irradiation time

of **8**. Each set of data is fit by $y = Ae^{-kt} + C$.

Figure S9. (a) 300 MHz ^1H NMR spectra of an 89.2 mm solution of **9** (CD_3CN) after 0 min (bottom), 30 min (middle) and 180 min (top) (b) Difference between 300 MHz ^1H NMR spectra of **9** (CD_3CN) before and after 180 min irradiation at 350 nm (c) Plot of decreasing ^1H NMR integrals scaled by initial integral and number of protons with increasing irradiation time of **9**. Each set of data is fit by $y = Ae^{-kt} + C$.

Table S1. Compounds with representative bond dissociation energies for the hydrogen atoms of **1**, the relation of each representative bond to **1** and the competitive rate value of k/k_a scaled for the number of hydrogen atoms.

Table S2. Compounds with representative bond dissociation energies for the hydrogen atoms of **2**, the relation of each representative bond to **2** and the competitive rate value of k/k_a scaled for the number of hydrogen atoms.

Table S3. Compounds with representative bond dissociation energies for the hydrogen atoms of **3**, the relation of each representative bond to **3** and the competitive rate value of k/k_a scaled for the number of hydrogen atoms.

Table S4. Compounds with representative bond dissociation energies for the hydrogen atoms of **4**, the relation of each representative bond to **4** and the competitive rate value of k/k_a scaled for the number of hydrogen atoms.

Table S5. Compounds with representative bond dissociation energies for the hydrogen atoms of **5**, the relation of each representative bond to **5** and the competitive rate value of k/k_a scaled for the number of hydrogen atoms.

Table S6. Compounds with representative bond dissociation energies for the hydrogen atoms of **6**, the relation of each representative bond to **6** and the competitive rate value of k/k_a scaled for the number of hydrogen atoms.

Table S7. Compounds with representative bond dissociation energies for the hydrogen atoms of **7**, the relation of each representative bond to **7** and the competitive rate value of k/k_a scaled for the number of hydrogen atoms.

Table S8. Compounds with representative bond dissociation energies for the hydrogen atoms of **8**, the relation of each representative bond to **8** and the competitive rate value of k/k_a scaled for the number of hydrogen atoms.

Table S9. Compounds with representative bond dissociation energies for the hydrogen atoms of **9**, the relation of each representative bond to **9** and the competitive rate value of k/k_a scaled for the number of hydrogen atoms.

REFERENCES

- Johnson, J. A., J. M. Baskin, C. R. Bertozzi, J. T. Koberstein and N. J. Turro (2008) Copper-free click chemistry for the in situ crosslinking of photodegradable star polymers. *Chem. Comm.* **26**, 3064–3066.
- von Raumer, M., P. Suppan and E. Haselbach (1996) Photoreduction of triplet benzophenone by amines: Role of their structure. *Chem. Phys. Lett.* **252**, 263–266.
- von Raumer, M., P. Suppan and E. Haselbach (1997) Photoreduction of triplet benzophenone by tertiary amines: Amine molecular structure and ketyl radical yield. *Helv. Chim. Acta* **80**, 719–724.
- Turro, N. J. (1991) *Modern Molecular Photochemistry*. University Science Books, Sausalito, CA.
- Visanathan, K., C. E. Hoyle, E. S. Jönsson, C. Nason and K. Lindgren (2002) Effect of amine structure on photoreduction of hydrogen abstraction initiators. *Macromolecules* **35**, 7963–7967.
- Carroll, G. T., M. E. Sojka, X. Lei, N. J. Turro and J. T. Koberstein (2006) Photoactive additives for cross-linking polymer films: Inhibition of dewetting in thin polymer films. *Langmuir* **22**, 7748–7754.
- Carbone, N. D., M. Ene, J. R. Lancaster and J. T. Koberstein (2013) Kinetics and mechanisms of radical-based branching/cross-linking reactions in preformed polymers induced by benzophenone and bis-benzophenone photoinitiators. *Macromolecules* **46**, 5434–5444.
- Finn, M., R. Friedline, N. K. Suleman, C. J. Wohl and J. M. Tanko (2004) Chemistry of the t-butoxyl radical: Evidence that most hydrogen abstractions from carbon are entropy-controlled. *J. Am. Chem. Soc.* **126**, 7578–7584.
- Tanko, J. M., R. Friedline, N. K. Suleman and N. Castagnoli (2001) Tert-butoxyl as a model for radicals in biological systems: Caveat emptor. *J. Am. Chem. Soc.* **123**, 5808–5809.
- Russell, G. A. (1973) Reactivity, selectivity, and polar effects in hydrogen atom transfer reactions. In *Free Radicals*, (Edited by J. K. Kochi), pp. 275–331. Wiley, New York, NY.
- Aleman, C., V. M. Domingo, L. Fajari, L. Julia and A. Karpfen (1998) Molecular and electronic structures of heteroaromatic oligomers: Model compounds of polymers with quantum-well structures. *J. Org. Chem.* **63**, 1041–1048.
- Ashton, P. R., J. Huff, S. Menzer, I. W. Parsons, J. A. Preece, J. F. Stoddart, M. S. Tolley, A. J. P. White and D. J. Williams (1996) Bis[2]catenanes and a bis[2]rotaxane-model compounds for polymers with mechanically interlocked components. *Chem. Eur. J.* **2**, 31–44.
- Bortolus, P., S. Dellonte and G. Beggato (1977) Interaction between singlet oxygen ($^1\Delta_g$) and model compounds for polymers. A flash photolytic study. *Eur. Polym. J.* **13**, 185–188.
- Allen, N. (2001) Photoinduced chemical crosslinking activity and photo-oxidative stability of amine acrylates: Photochemical and spectroscopic study. *Polym. Degrad. Stabil.* **73**, 119–139.
- Mintsa, M. N., L. Lecamp, C. Loutelier-Bourhis, C. M. Lange, S. Baumgarten and C. Bunel (2009) Photocrosslinking of a novel α , ω -unsaturated copolyamide: Mass spectrometric study on model compounds with benzophenone as photoinitiator. *Rap. Comm. Mass Spectrom.* **23**, 3813–3823.
- Montalti, M., L. Prodi, A. Credi and M. T. Gandolfi (2006) *Handbook of Photochemistry*, 3rd ed. CRC/Taylor & Francis, New York.
- Luo, Y.-R. (2003) Tabulated BDEs of O–X bonds. In *Handbook of Bond Dissociation Energies in Organic Compounds*, pp. 163–231. CRC Press LLC, Boca Raton.
- Luo, Y.-R. (2003) Tabulated BDEs of C–H bonds. In *Handbook of Bond Dissociation Energies in Organic Compounds*, 11–93. CRC Press LLC, Boca Raton.
- Luo, Y.-R. (2003) Tabulated BDEs of N–X bonds. In *Handbook of Bond Dissociation Energies in Organic Compounds*, 232–270. CRC Press LLC, Boca Raton.
- Tumanov, V. E. and E. T. Denisov (2001) Evaluation of C–H bond dissociation energies in hydrocarbons and the enthalpies of the relevant radicals from kinetic data. *Petr. Chem.* **41**, 109–118.
- Kerr, J. A. (1966) Bond dissociation energies by kinetic methods. *Chem. Rev.* **66**, 465–500.
- van Speybroeck, V., G. B. Marin and M. Waroquier (2006) Hydrocarbon bond dissociation enthalpies: From substituted aromatics to large polyaromatics. *Chem. Phys. Chem.* **7**, 2205–2214.
- Watts, Z. I. and C. J. Easton (2009) Peculiar stability of amino acids and peptides from a radical perspective. *J. Am. Chem. Soc.* **131**, 11323–11325.
- Scheiner, S. and T. Kar (2010) Analysis of the reactivities of protein C–H bonds to H atom abstraction by OH radical. *J. Am. Chem. Soc.* **132**, 16450–16459.